Check for updates

A distinct correlation between the vibrational and thermal transport properties of group VA monolayer crystals†

Tuğbey Kocabaş,[a] Deniz Çakır,[b] Oğuz Gülseren,[c] Feridun Ay,[d] Nihan Kosku Perkgöz[d] and Cem Sevik [ID] *[e]

The investigation of thermal transport properties of novel two-dimensional materials is crucially important in order to assess their potential to be used in future technological applications, such as thermoelectric power generation. In this respect, the lattice thermal transport properties of the monolayer structures of group VA elements (P, As, Sb, Bi, PAs, PSb, PBi, AsSb, AsBi, SbBi, P_3As_1, P_3Sb_1, P_1As_3, and As_3Sb_1) with a black phosphorus like puckered structure were systematically investigated by first-principles calculations and an iterative solution of the phonon Boltzmann transport equation. Phosphorene was found to have the highest lattice thermal conductivity, κ, due to its low average atomic mass and strong interatomic bonding character. As a matter of course, anisotropic κ was obtained for all the considered materials, owing to anisotropy in frequency values and phonon group velocities calculated for these structures. However, the determined linear correlation between the anisotropy in the κ values of P, As, and Sb is significant. The results corresponding to the studied compound structures clearly point out that thermal (electronic) conductivity of pristine monolayers might be suppressed (improved) by alloying them with the same group elements. For instance, the room temperature κ of PBi along the armchair direction was predicted to be as low as 1.5 W m^{-1} K^{-1}, whereas that of P was predicted to be 21 W m^{-1} K^{-1}. In spite of the apparent differences in structural and vibrational properties, we peculiarly revealed an intriguing correlation between the κ values of all the considered materials as $\kappa = c_1 + c_2/m^2$, in particular along the zigzag direction. Furthermore, our calculations on compound structures clearly showed that the thermoelectric potential of these materials can be improved by suppressing their thermal properties. The presence of ultra-low κ values and high electrical conductivity (especially along the armchair direction) makes this class of monolayers promising candidates for thermoelectric applications.

1. Introduction

Triggered by the rediscovery of black phosphorus (BP), group VA materials, specifically monolayer arsenic (As) and antimony (Sb), have started to receive attention due to their peculiar thermal, optical and electronic properties.[1–6] In fact, this excitement among different researchers is inspired by the fabrication of the first phosphorene (P monolayer) based transistor in 2014.[7] The

interest not only spreads to the optical and electronic communities but also to the research groups studying thermal properties.[2,8–10] From the optical and electronic points of view, phosphorene is appealing because of its high carrier mobility and direct band gap.[11] This band gap is also found to vary progressively from 0.3 eV to 2 eV when its thickness is reduced from its bulk form to single-layer form. On the other hand, the relatively low thermal conductivity and its directional dependency due to the anisotropic lattice structure in particular for phosphorene (P monolayer) and arsenene (As monolayer) are of immense value for thermoelectric applications, providing higher electro-thermal conversion efficiency.[2,8,12] Hence, materials with such properties present high potential to start a new line of research and development leading to completely new technologies.

Group VA elements have the electronic configuration of s^2p^3 in the outermost shell, where this sp^3 bonding causes a non-planarity, either a puckered or buckled structure.[9,13,14] van der Waals forces hold the 2D layers where each atom in a layer is 3-fold coordinated with covalent bonds.[15] The puckered struc-

[a]Department of Advanced Technologies, Graduate School of Sciences, Anadolu University, Eskisehir, TR 26555, Turkey
[b]Department of Physics and Astrophysics, University of North Dakota, Grand Forks, North Dakota 58202, USA
[c]Department of Physics, Bilkent University, Bilkent, Ankara 06800, Turkey
[d]Department of Electrical and Electronics Engineering, Faculty of Engineering, Anadolu University, Eskisehir, TR 26555, Turkey
[e]Department of Mechanical Engineering, Faculty of Engineering, Anadolu University, Eskisehir, TR 26555, Turkey. E-mail: csevik@anadolu.edu.tr
†Electronic supplementary information (ESI) available. See DOI: 10.1039/C7NR09349G
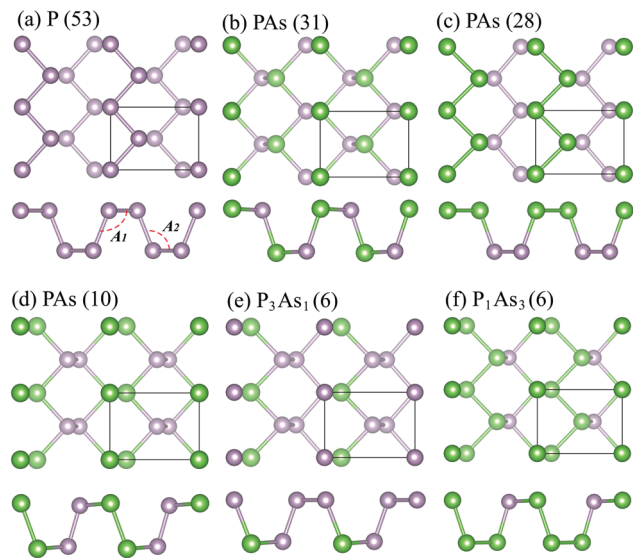
Fig. 1 Top and side views of the considered two-dimensional compounds with different space group symmetries, *Pmna*, *Pmn*2_1, *Pma*2, *P2/m*, and *Pm*.

tures of P, As, and Sb have been reported to be thermodynamically stable with high electron/hole mobility[16] and low thermal conductivity[17] values, which is essential for high-performance innovative thermoelectric research. Therefore, it is very motivating to spend more intense theoretical effort on the nature of phonon transport in these materials in order to shed light on their lattice thermal transport properties. In addition, low thermal conductivity of the VA column inspires controlling the thermal transport properties by material engineering such as using the alloys of these elements. Hence, in this study, it is also an object of interest regarding the change in thermal conductivity when group VA elements are considered as compound structures.

Therefore, we calculate the intrinsic lattice thermal conductivity of 21 stable single layer two-dimensional black phosphorane like structures shown in Fig. 1: P and As with the *Pmna* space group symmetry, Sb and Bi with the *Pmn*2_1 space group symmetry, PAs with the *Pma*2 space group symmetry, PAs, PSb, PBi, AsSb, AsBi, and SbBi with the *Pmn*2_1 and *P2/m* space group symmetries, and P_1As_3, P_3As_1, P_3Sb_1, and As_3Sb_1 with the *Pm* space group symmetry.

2. Methods

The structural and dynamical properties of all the considered systems were predicted by first-principles calculations based on density functional-theory (DFT) and density-functional perturbation theory (DFPT), as implemented in the Vienna *Ab initio* Simulation Package (VASP) code.[18–20] The exchange–correlation interactions were treated using the generalized gradient approximation (GGA) within the Perdew–Burke–Ernzerhof (PBE) formulation.[21,22] The single electron wave functions were expanded in plane waves with a kinetic energy cutoff of at

least 450 eV. For structure optimizations, the Brillouin-zone integrations were performed using a Γ-centered regular 21 × 21 × 1 *k*-point mesh within the Monkhorst–Pack scheme.[23] The convergence criteria for electronic and ionic relaxations were set as 10^{-7} eV and 10^{-3} eV Å^{-1}, respectively. In order to minimize the periodic interaction along the *z*-direction the vacuum space between the layers was taken at least 15 Å.

Lattice thermal transport properties were determined using the self-consistent solution of the Peierls–Boltzmann transport equation[24] as implemented in the ShengBTE code.[25,26] The zeroth iteration solutions corresponding to Relaxation Time Approximation (RTA) were also predicted in order to clarify the influence of the quasi-momentum-conserving normal and the non-quasi-momentum-conserving Umklapp scattering processes on the thermal transport results. The second-order inter-atomic force constants (IFCs) required by the ShengBTE were obtained using the PHONOPY code which extracts the appropriate force-constant file from the results predicted by DFPT as implemented in the VASP. The third-order IFCs were derived from the VASP calculations of the structures generated by considering up to 10 next-nearest-neighbor interactions. Here, 8 × 8 × 1 and 5 × 5 × 1 supercell structures were used in the DFT calculations performed to predict the second- and third-order IFCs, respectively. In lattice thermal transport calculations, at least 40 × 40 × 1 well converged *q*-grid and an out of plane lattice constant *d* = 5.36 Å^{27,28} were used for all the considered single layer materials.

3. Results

The primitive unit cell of the considered four pristine (P, As, Sb and Bi), thirteen binary compound (PAs, PSb, PBi, AsSb, AsBi, and SbBi) and six one-third compound (P_3As_1, P_3Sb_1, P_1As_3, and As_3Sb_1) group VA monolayer crystals has a rectangular lattice with a four-atom basis and distinctive space group symmetries, namely *Pmna* (53), *Pmn*2_1 (31), *Pma*2 (28), *P2/m* (10), and *Pm* (6), see Fig. 1. Therefore, except for the three acoustic modes involving the in-phase vibrations of atoms in the unit cell, the out-of-phase vibrations of the atoms give rise to nine optical modes for all the structures. The calculated phonon dispersion curves, corresponding to these modes, are depicted in ESI, Fig. 2, 3, and 4,† respectively, together with the group velocity of each phonon mode as a line color. As seen in these figures, no negative frequencies, indicating the dynamical instability at *T* = 0 K, were found for most of the considered structures. However, appreciable negative frequencies for the PSb, PBi, AsSb, AsBi, and SbBi structures with the *Pma*2 space group symmetry were obtained, which means that these structures are not dynamically stable. Also, a few THz negative frequencies for P_1Sb_3 and As_1Sb_3 with the *Pm* space group symmetry were found and these structures were not considered in thermal transport calculations. The in-plane longitudinal acoustic (LA) and transverse acoustic (TA) modes of all the materials have a linear dependence as *q* becomes zero (*i.e.* long wavelength limit), whereas the out-of-plane acoustic or flexural modes (ZA) have a quadratic dependence on the long wavelength limit as commonly observed
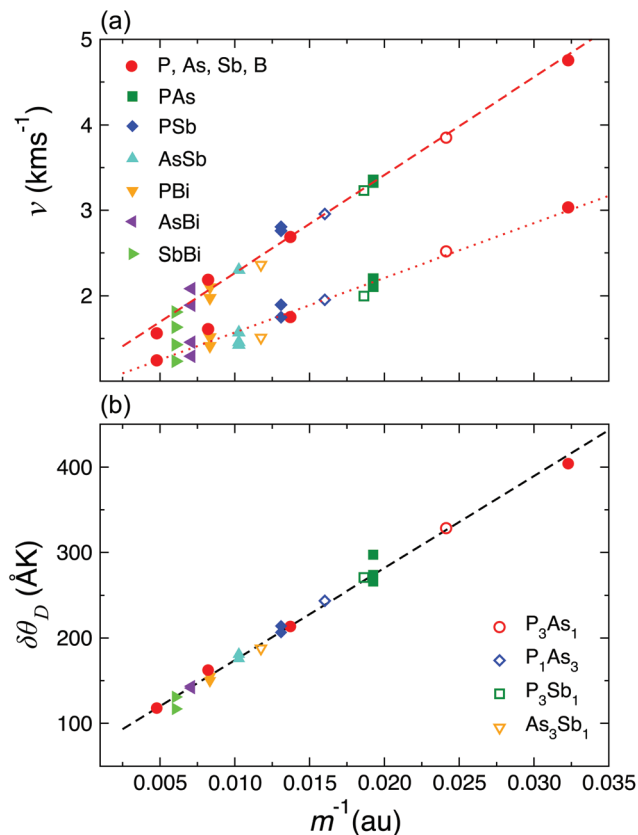
Fig. 2 (a) The calculated average acoustic mode group velocities, v, along the ZZ and AC directions *versus* m^{-1}. Here, m is the average atomic mass of the unit cell. The red dashed and dotted lines represent the linear fitting values along the ZZ and AC directions, respectively. (b) $\delta\theta_D$ *versus* m^{-1}, where δ^2, θ_D, and m are the area of the unit cell per atom, Debye temperature, and average atomic mass of each system, respectively. The black dashed line shows the linear fitting values.

in two-dimensional (2D) materials such as graphene. The considered compounds display different dispersion curves with distinctive Debye frequencies, resulting in different phonon group velocity $\left(v_{qi} = \dfrac{\partial\omega_{qi}}{\partial q}\right)$ values. Fig. 2(a) shows the calculated average of group velocities of three acoustic modes along the zigzag (ZZ) and armchair (AC) directions (corresponding to the reduced reciprocal coordinates, $q_x = 0.05$, $q_y = 0.00$ for ZZ, and $q_x = 0.00$, $q_y = 0.05$ for AC). A simple correlation between the average of group velocities of three acoustic modes, v, and the average effective mass of elemental configuration of the unit cell, m, was established as $v = c_1 + c_2/m$, where c_1 and c_2 are constants. Our simple expression is consistent with the fact that the lower the average mass, the higher the group velocity.

The maximum frequency (ω_m) values at the Γ-point change as $\omega_{m,P} > \omega_{m,As} > \omega_{m,Sb} > \omega_{m,Bi}$ and $\omega_{m,PAs} > \omega_{m,P3As_1} > \omega_{m,PAs_1},\dots, > \omega_{m,SbBi}$ mainly due to the bond stiffness, different atomic masses for pristine monolayers and average atomic mass of the unit cell for the alloy monolayers. When the bond stiffness becomes weaker (*i.e.* interatomic force constant becomes smaller) and the mass of the atom becomes larger, the phonon

frequencies shift to lower energies. Thus, the phonon branches become less disperse with exactly the same order, and v_{qi} values of phonon modes markedly decrease with increasing the mass of the constituent atom(s). In this context, the Debye temperature, calculated from the contributions of individual acoustic modes (*i.e.* $\theta_i = \hbar\omega_{i,max}/k_B$, where i = LA and TA) is given as[29]

$$\frac{1}{\theta_D^3} = \frac{1}{2}\left(\frac{1}{\theta_{LA}^3} + \frac{1}{\theta_{TA}^3}\right). \quad (1)$$

The calculated Debye temperature (θ_D) values for all the considered monolayer materials are listed in Table I in the ESI.† While θ_D is 206 K for phosphorene, it becomes 50 K for Bi. For 2D crystals, the Debye temperature can also be defined as follows:[30]

$$\theta_D = \frac{\hbar v_s}{k_B}\left(\frac{4\pi n}{A}\right)^{1/2}, \quad (2)$$

where v_s is the velocity of sound, n is the number of atoms in the unit cell, and A is the area of the unit cell.[14] Based on this formula, we calculated the square root of the unit cell area per number of atoms, $\delta^2 = A/n$, times Debye temperature (calculated from phonon dispersion *via* eqn (1)) with respect to the inverse average atomic mass of the crystals (*i.e.* total atomic mass over the number of atoms in the unit cell, m/n). Quite surprisingly, the predicted Debye temperatures from our calculations are correlated with the lattice constants and inverse of the average atomic mass as expected from eqn (2), see Fig. 2(b). Note that, the velocity of sound in the plot is considered as inversely proportional to the average mass as it is in anharmonic crystals and our results shown in Fig. 2(a) clearly prove these relationships. The obtained perfect m^{-1} correlation in both v and θ_D indicates that these systems might be quite anharmonic.

The phonon dispersion curves shown in the ESI† are not symmetric along the Γ–X–S and Γ–Y–S, giving rise to anisotropic phonon group velocities along the zigzag and armchair directions. In fact, all the considered monolayers resemble the orthogonal symmetry resulting in distinctive interatomic bonding structures along the ZZ and AC directions, which induces anisotropic vibrational properties. Interestingly, the dispersion of acoustic modes along the ZZ and AC directions for the Sb and Bi structures is not so different compared to the P and As structures, which would give rise to a smaller difference in thermal conductivity along the ZZ and AC directions. The predicted group velocities of the LA modes of phosphorene along the ZZ and AC directions (see Fig. 2 in the ESI†) are in a good agreement with the previously reported first-principles results (8.6 and 4.5 km s^{-1})[10] and experimental measurements (9.6 and 4.6 km s^{-1})[31] for bulk black phosphorus. The acoustic modes travel at a higher speed along the ZZ direction since all the monolayers are stiffer along the ZZ direction compared to the AC direction. Note that the v_{qi} values of the major heat carrier phonon branches, *i.e.* the acoustic modes of Sb and Bi along both the ZZ and AC directions near the zone center are about two times smaller than those of black phosphorus as seen in Fig. 2(a). This notable difference in the group velocity values

of acoustic branches is fairly associated with the difference in the κ values of these crystals.

In principle, we have four kinds of three-phonon scattering processes, including a + a ↔ a, a + a ↔ o, a + o ↔ o and o + o ↔ o, where a and o stand for acoustic and optical phonon modes, respectively. The phonon scattering depends on the number of available channels, which can directly be determined from the phonon dispersion plots. The frequency gaps between the 3 low frequency optical phonons and the remaining 6 high frequency optical phonons are around 2 THz for P and As and less than 1 THz for Sb and Bi. The presence of a frequency gap between the low frequency and high frequency optical branches of most of the considered structures might have an effect on the thermal transport properties of these materials. According to the selection rule of three phonon scattering processes, total energy ($\omega \pm \omega' = \omega''$) and momentum ($q \pm q' = q'' - \mathbf{G}$, where $\mathbf{G}$ is the reciprocal lattice vector) of phonons involved in the scattering process are required to be conserved. This means that the presence of the frequency gap indicates the suppressed scattering channels for phonons, thereby giving rise to longer mean free paths for phonons, and therefore higher lattice thermal conductivity. In fact, in the former studies, the lower thermal conductivity of puckered phosphorus compared to buckled phosphorus is correlated with the presence of a larger a–o gap in the buckled one.[9] The absence of the a–o gap provides more channels for the scattering of acoustic modes into optical modes. Also, the significant effect of acoustic–optical phonon gaps on the a + a ↔ o scattering channels was shown for different low-dimensional materials.[9,32–34] These above-mentioned three phonon processes may also affect the temperature dependence of κ since as the temperature increases, the number of optical phonons increase thereby enhancing three phonon processes involving optical phonons. There is a notable difference in the phonon dispersions of the compound monolayers with the same concentration but different symmetry, see for example, Fig. 3 in the ESI† for the phonon dispersion curves of PSb with symmetries $Pmn2_1$ and $P2/m$. Therefore, we can expect distinctive phonon scattering mechanisms in the compounds with different symmetries.

Subsequent to the phonon dispersion analysis, we first calculated the lattice thermal conductivity of graphene in order to test our methodology and we predicted it as 3290 W m^{-1} K^{-1} which is in quite good agreement with the literature[35–38] (shown in ESI, Fig. 5†). Afterwards, we systematically investigated the lattice thermal transport properties of four pristine, thirteen binary and four one-third group VA monolayer structures. The self-consistent solutions of the Peierls–BTE for the lattice thermal conductivity (κ) of the pristine monolayers as a function of temperature in the range of 100 K to 600 K are shown with colored symbols in Fig. 3(a) and (b). The κ value decreases along both the ZZ and AC directions when moving from P to Bi. Phosphorene has the highest κ value due to its highest θ_D temperature. We found that all the monolayers exhibit obvious anisotropic thermal transport, mainly attributed to the anisotropic phonon dispersion,[39–41] which leads to direction-dependent group velocities, as clearly seen in Fig. 2(a).
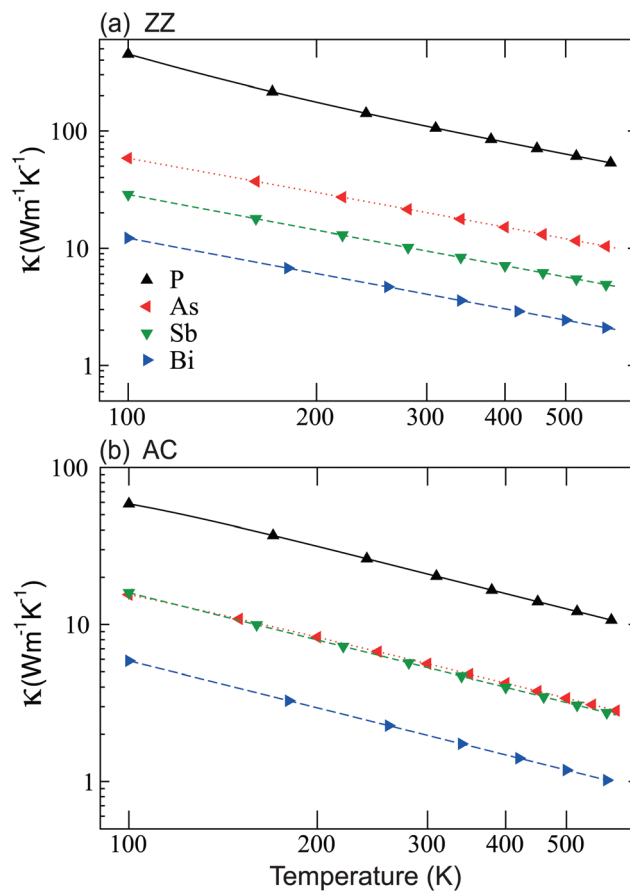

Fig. 3 Thermal conductivity of group VA monolayer crystals as a function of temperature along the (a) zigzag and (b) armchair directions obtained from the self-consistent solution of the Peierls–BTE.

We found that all the monolayers exhibit obvious anisotropic thermal transport, which is mainly attributed to the anisotropic phonon dispersion,[39–41] which leads to direction-dependent group velocities, as clearly seen in Fig. 2(a). For instance, the room temperature κ along the ZZ direction is 5.21, 3.63, 1.78, and 2.05 times larger than that along the AC direction for P, As, Sb, and Bi, respectively. Interestingly, this ratio, which is nearly the same for Sb and Bi, changes linearly with the atomic mass of P, As, and Sb. This behavior is consistent with the recent theoretical studies[9,10,40,42,43] performed using first-principles calculations, see Table 1.

Previously, the thermal conductivity of a few layer black phosphorus film with 15 nm thickness was measured to be 40 and 20 W m^{-1} K^{-1} and a film with 9.5 nm thickness was measured[2] to be 20 and 10 W m^{-1} K^{-1} along the ZZ and AC directions, respectively. In addition, the thermal conductivity of a single crystal bulk black phosphorus was measured[41] to be 34 and 17 W m^{-1} K^{-1} along the ZZ and AC directions, respectively. Even though we cannot directly compare the κ value of a monolayer material with that of its few-layer and bulk forms, our results for the κ value of phosphorene along both the directions are in fair accordance with the previously
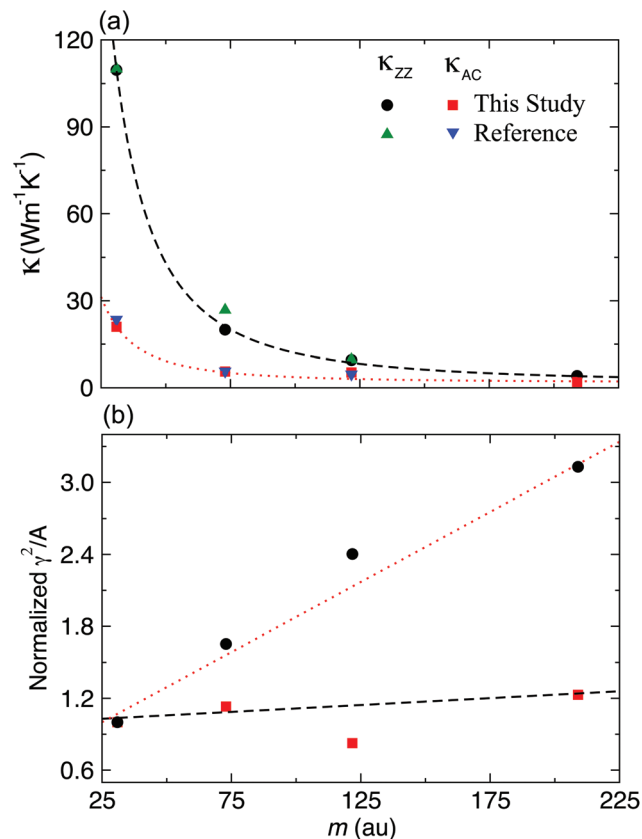
Table 1 The calculated room temperature κ values of the monolayer structures (bold faces), together with the results reported in the literature. *a*, *b*, *c*, *d*, *e*, *f*, *g*, and *h* correspond to the results extracted from ref. 9, 44, 42, 8, 43, 40, 10, and 45, respectively. Here, the values are rescaled with the out of plane lattice constant. 5.36 Å (corresponding to the interlayer distance in bulk black phosphorus) was used in our study to make a reliable comparison of the monolayer structures with each other. The out of plane lattice constant values are not available for the results represented with bold italic face

P		As		Sb		Bi	
κ_{ZZ}	κ_{AC}	κ_{ZZ}	κ_{AC}	κ_{ZZ}	κ_{AC}	κ_{ZZ}	κ_{AC}
109.6	**21.0**	**20.3**	**5.6**	**9.6**	**5.4**	**4.5**	**2.7**
109.9[a]	23.5[a]	26.8[a]	5.7[a]	9.7[a]	4.7[a]	7.8[b]	6.0[b]
30.2[c]	*13.6[c]*	*30.4[d]*	*7.8[d]*				
48.9[e]	*27.8[e]*						
107.7[f]	35.3[f]						
81.6[g]	23.8[g]						
15.3[h]	4.6[h]						

reported experimental data for bulk and few-layer systems in terms of order of magnitude. Our calculated κ value of phosphorene is probably higher than that of the phosphorene film with a thickness of 9.5 nm due to the strong interlayer interaction in the measured multilayer samples. The overlap of interlayer wavefunctions rather than a pure van der Waals interaction[46,47] leads to an interlayer interaction much stronger than graphene in this crystal. In addition, the thermal conductivity of phosphorene was calculated by several groups. Interestingly, there is a deviation between the calculated κ values as seen in Table 1. This can partially be attributed to different computational methods and computational parameters used in these studies. The calculated values for P, As, and Sb structures in this study agree very well with the values reported in a recent study.[9]

Our calculations revealed that there is a distinct correlation between the κ value of pristine P, As, Sb, and Bi structures and average atomic mass (m). We found a simple correlation between m and $\kappa(m)$ such that $\kappa(m) = c_1 + c_2/m^2$, where c_1 and c_2 are constants, see Fig. 4(a). Not surprisingly, the thermal conductivity values predicted by Zheng *et al.* also fit this function very well. In addition to this surprising correlation, we predicted that the κ values of all the pristine monolayers follow nearly the same trend with temperature as seen in Fig. 3. Therefore, we can certainly claim that the decrease in the κ values of the pristine structures (*i.e.* P, As, Sb, and Bi) at temperatures above 100 K follows a m^{-2} behavior except for the slight deviation in the κ value of Sb along the AC direction. In fact, the space group symmetry of P and As is different from that of Sb and Bi due to the different bond bending angles, A_1 and A_2 shown in Fig. 1 and thus one can naturally expect distinctive thermal transport properties for these two groups. Consequently, the marked correlation revealed as a result of our calculations is quite remarkable.

Previously, Slack suggested that the thermal conductivity (κ_s) is determined by four factors, including (1) average atomic

Fig. 4 (a) Calculated room temperature κ values of the P, As, Sb, and Bi based structures, together with the results reported in ref. 9 and (b) the γ^2/A as a function of average atomic mass. Here, the black circles and red squares show the values calculated in this study and the green up and blue down triangles show the values reported in the literature.[9] The black dashed and red dotted lines in (a) correspond to the fitted values (*i.e.* $\kappa(m) = c_1 + c_2/m^2$) along both the directions.

mass, (2) interatomic bonding, (3) crystal structure and (4) size of anharmonicity.[48] The first three factors determine harmonic properties. Three phonon scattering dominated κ_s values can be given as

$$\kappa_s = A\frac{m\theta_D{}^3\delta n^{1/3}}{\gamma^2 T} \qquad (3)$$

where δ^2 is the unit-cell area per atom, n is the number of atoms in the unit cell (which is equal to four for all systems), A is a constant given in terms of average Grüneisen parameter of modes,[29] γ, and m is the average atomic mass of the unit cell. Here, the degree of anharmonicity is characterized by the size of the Grüneisen parameter. The larger the Grüneisen parameter of mode, the stronger the anharmonicity. In other words, larger anharmonicity means the more frequent scattering of a phonon mode by other phonon modes. We used this equation to predict the size of anharmonicity in these systems. First of all, this simple relationship neglects the contribution of the optical modes to the thermal conductivity. This is a reasonable approximation since the contribution of the optical modes to thermal conductivity does not exceed 10% for most

of the considered crystals as shown in the ESI.† Inspired from the above relationship, we calculated the γ^2/A as,

$$\frac{m\theta_D{}^3\delta n^{1/3}}{\kappa T}, \tag{4}$$

at 300 K. Here, we used the κ values shown in Fig. 4. Then, the results were normalized by the calculated κ value of P. Within the Slack's approximation, the γ^2/A term is directly related to the anharmonicity of the crystal (the larger the γ, the larger the anharmonic effect). In this work, we did not explicitly calculate the γ. However, we can safely claim that the γ is strongly correlated with the mass of atoms. Our calculations clearly show that there is a notable difference between the anharmonic effects along the ZZ and AC directions. While there is a steep increase in the ZZ direction, the values along the AC direction are very close to each other, and the calculated value for Sb is even smaller than that of P.

Fig. 5 shows the calculated lattice thermal transport properties of thirteen binary, (a), (b), and four one-third, (c), (d), group VA monolayer structures. Not surprisingly, all the considered compound monolayer crystals exhibit an obvious anisotropic thermal transport, which is mainly attributed to the orientation dependent group velocities seen in Fig. 2(a). The compound monolayers containing P have larger thermal conductivity compared with the compounds without P atoms. The monolayers with Bi have the lowest thermal conductivities for all temperature values considered here. For instance, the κ value of PBi with the $P2/m$ space group was found to be 1.5 W m^{-1} K^{-1}. The calculated κ values of low symmetry compound systems, as low as the κ values of well-known 2D thermoelectric materials including single layer SnSe (0.46–0.70 W m^{-1} K^{-1} at 300 K),[49] clearly show that the thermal conductivity of pristine systems can be suppressed up to an order of magnitude by alloying in a controllable manner. Indeed, random elemental distribution in alloy systems results in significant reduction in the phonon mean free path of long wavelength heat carrier phonons.[50,51] Therefore, it can be reasonably proposed that the κ value of black phosphorus can be tuned (reduced to enhance its thermoelectric potential) by alloying it with Sb, Bi, and also As doping even with very low doping concentrations,[36,52] that will lead to an opportunity to
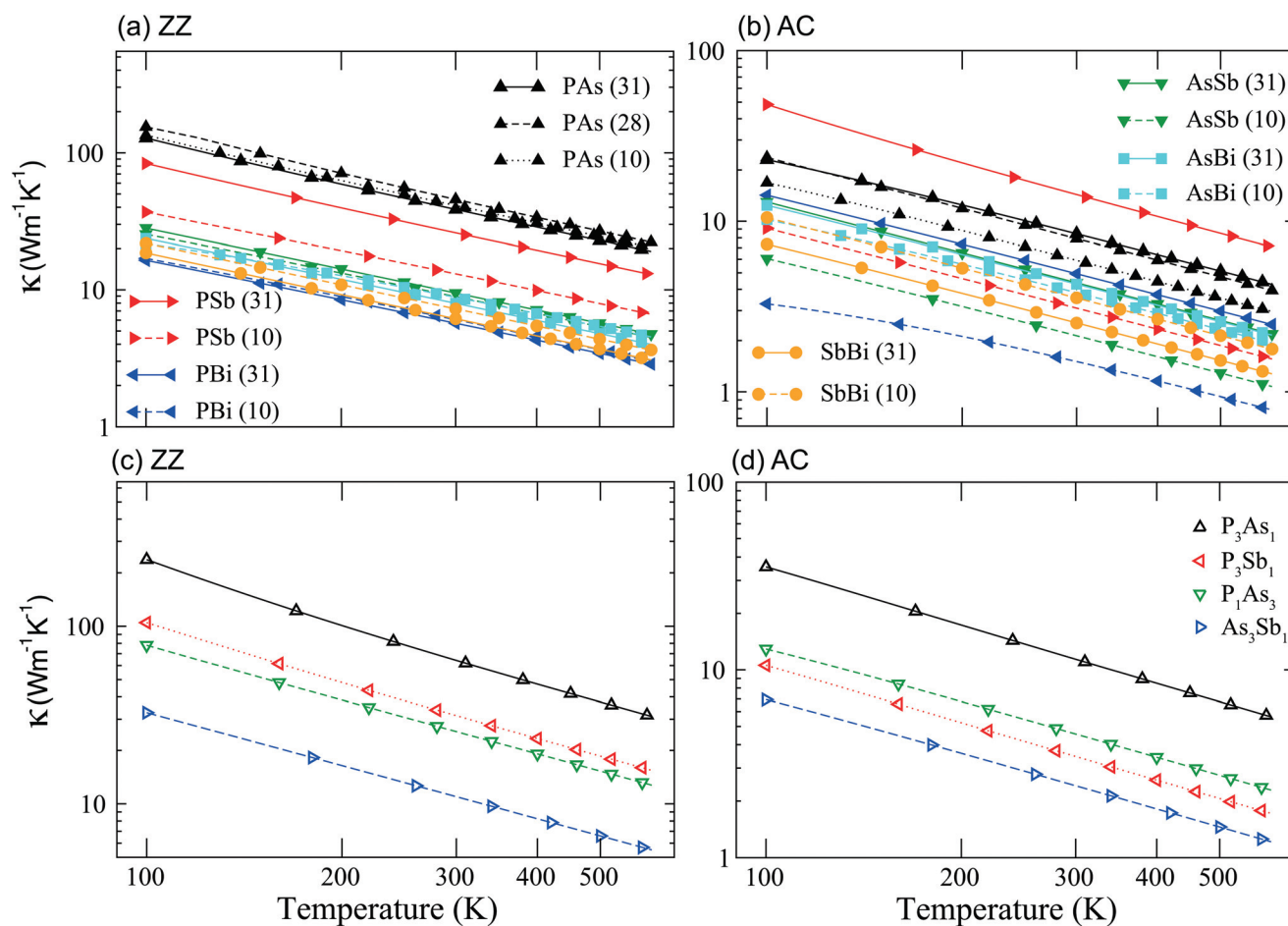

Fig. 5 Thermal conductivity of stable group VA compound crystals with all the possible crystal symmetries as a function of temperature along the (a), (c) zigzag and (b), (d) armchair directions calculated by the self-consistent solution of the Peierls−BTE. Numbers in parentheses show the space groups.

engineer these materials. This is because of the fact that substitutional As, Sb or Bi doping improves (suppresses) the electronic (thermal) transport by increasing (decreasing) the density of states around the Fermi level (band gap), see Fig. 6–8 in the ESI.† In addition, most of the monolayer structures considered here exhibit multiple extrema in their valence and conduction bands, mainly originating from multiple bands. For instance, the edges of the valence bands yield several hole pockets. These extrema in the valence and conduction bands are nearly energetically degenerate with the energy difference less than 0.15 eV and they are all accessible by doping. These types of electronic features in the electronic band structure may give rise to large Seebeck coefficients in these monolayer structures. In other words, these extrema can collectively contribute to the overall Seebeck coefficient and the power factor. SnSe possesses a complex electronic band structure akin to our alloy group VA monolayers. This complexity is one of the reasons for the enhanced thermoelectric performance of this material.[53] For the low band gap systems, bipolar conduction may emerge at high temperatures, which lowers the Seebeck coefficient. The optimum band gap value for a good thermoelectric material is around $10k_BT$.[54] The considered monolayer structures have band gap values within the range of 0.09–0.9 eV. Depending on the application temperature range, we can maximize thermoelectric efficiency by selecting appropriate monolayers. A combination of the ultralow κ value and high electrical conductivity makes these monolayers promising candidates for thermoelectric applications. In our calculations, we did not include spin–orbit coupling (SOC). In fact, SOC becomes more effective for the monolayer structures with heavy atoms, such as Bi. It was shown that SOC has a non-negligible effect on the electronic properties of the Bi monolayer.[55] However, we do not expect a significant impact of SOC on phonons and thermal conductivity values. For the calculations of conductivity and Seebeck coefficient, SOC should be taken into account to obtain accurate results.

The correlation between the κ values of pristine P, As, Sb, and Bi monolayers and their compound structures with average atomic mass was also investigated for all the considered materials. Here, the κ value for a compound structure was calculated as average over the κ values corresponding to all the considered symmetries of an individual concentration. As seen in Fig. 6(a), the $\kappa(m) = c_1 + c_2/m^2$ curve fits quite well with the calculated κ values along the ZZ direction of all the considered materials. However, the calculated κ values along the AC direction of P_3Sb_1, PSb, As_3Sb_1, and Sb do not follow the same relationship as good as along the ZZ direction as seen in Fig. 6(b). Nevertheless, when these results were considered with the identical temperature dependency of the κ values of all the materials presented in Fig. 5, it can be clearly stated that the κ values of compound group VA monolayer structures can be definitely estimated with the $\kappa(m) = c_1 + c_2/m^2$ relationship, above 100 K, with less than 10% error, except for 36% and 42% underestimation for the κ values of Sb and PSb, and 128% and 89% underestimation for the κ values of P_3Sb_1 and As_3Sb_1. Despite the apparent differences, such as group velo-
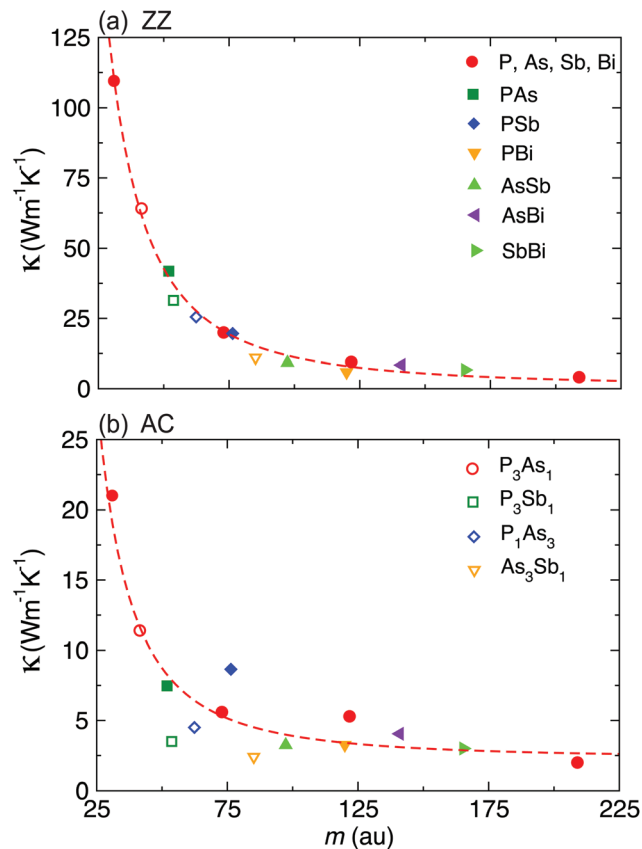

Fig. 6 (a) Calculated room temperature κ values of the group VA pristine and compound crystals along the (a) zigzag and (b) armchair directions. The red dashed lines represent the $c_1 + c_2/m^2$ fitting values.

cities and optical phonon gap values, in phonon dispersion of these materials, the revealed simple trend is quite striking.

The normalized γ^2/A values are also calculated for the compound structures. As observed for the pristine monolayers, there is no obvious trend with average atomic mass as shown in Fig. 7(a). However, it can be partially asserted that the normalized conductivity along the ZZ direction increases with increasing average mass, which means that the effect of anharmonicity becomes more and more prominent. However, the values along the AC direction scatter without an explicit trend. Interestingly, the change in the lattice parameters along the ZZ, a_0 and AC, b_0 directions, is in line with these results as shown in Fig. 8. This partially indicates that the change in some structural parameters, such as A_1, A_2 and A_3 angles depicted in Table V in the ESI,† due to the change in the electronic–ionic bonding nature (i.e. P–P is different from the Sb–Sb bond), leads to a distinctive direction dependent phonon group velocity and scattering rate values in these monolayer structures. This interpretation is also supported by the mean free path, l, dependent thermal conductivities shown in Fig. 9, 10, and 11 in the ESI.† For instance, the mean free paths of Sb and PSb along the AC direction are considerably longer than those along the ZZ direction. Conversely, the l of P, Bi, and PAs ($Pma2$) along the ZZ direction are rather larger.
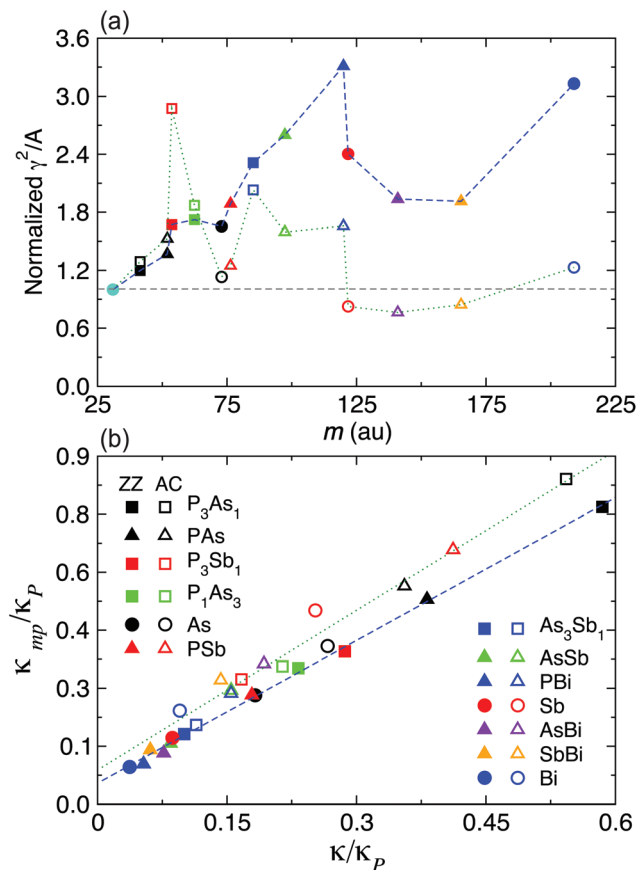
Fig. 7 (a) The calculated γ^2/A values *versus* average atomic mass, m and (b) κ/κ_P *versus* κ_{mp}/κ_P for pristine and compound crystals. The blue dashed (solid symbols) and green dotted (open symbols) lines connect the values calculated along the zigzag and armchair directions, respectively.
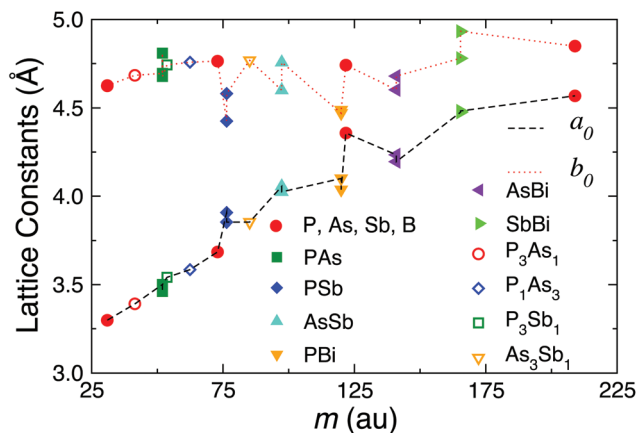

Fig. 8 Calculated lattice parameters along the ZZ (a_0) and AC (b_0) directions.

As mentioned above, Slack suggested that the thermal conductivity is determined by four factors.[48] In this regard, in order to differentiate the effects of purely interatomic bonding and size of anharmonicity on the thermal conductivity of the crystals, we recalculated the thermal conductivity of all the considered monolayers by equating the mass of all the constituent elements to the mass of phosphor (called κ_{mp}). Afterwards, we calculated the ratio of the actual conductivity, κ, and the one obtained with the mass of phosphor, κ_{mp} to the thermal conductivity of P, κ_P, as shown in Fig. 7(b). The deviation of κ_{mp}/κ_P from unity depicts the effects of the interatomic bonding and anharmonic interactions on the thermal conductivity. In other words, it shows a difference in the strength of interatomic bonds, which results in distinctive vibrational properties and thus anharmonic nature, of all the considered materials. The results for the ZZ direction show that these two effects dominate more and more the lattice thermal transport as the average mass of the unit cell decreases. However, such correlation for the AC direction is not as strong as that for the ZZ direction. These results clearly point out the dependence of anharmonicity on the crystal direction.

The zeroth iteration solutions of the Peierls–BTE corresponding to RTA were also calculated. The former is able to capture simultaneous interaction of all phonon modes, giving rise to collective phonon excitation being responsible for heat transfer. The ratios of the self-consistent iterative solution to RTA solution for both the ZZ and AC directions are depicted in Fig. 9, 10, and 11 in the ESI,† respectively. The difference between the self-consistent and RTA results is greater than 10% and independent of temperature when the temperature is slightly greater than the θ_D temperature of the monolayers. This clearly shows that the normal three-phonon processes play an important role in most of the compound crystals investigated in this study. For the 3D crystals with strong Umklapp scattering, room temperature calculated with the iterative solution is typically 10% greater than the RTA solution[56] and the difference between the two methods becomes considerably large for 2D materials. The RTA always severely underestimates thermal conductivity when the normal scattering (being dominant at low T) is strong. The κ values of all the structures are almost inversely proportional to the temperature ($\kappa \sim T^{-1}$), indicating that the phonon scattering mechanism is dominated by the Umklapp process. We found that the dominant scattering mechanism along the ZZ and AC directions is notably different from each other in particular for the structures with P atoms. For instance, the calculated ratio for the pristine P and As structures along the ZZ direction is larger than 1.8, however, the one obtained for the AC direction is smaller than 1.2. The calculated results for pristine Sb explicitly indicate that Umklapp scattering in this structure is considerably stronger than the other pristine ones in particular along the AC direction. This may explain the slight deviation in the κ value of Sb from the $\kappa(m) = c_1 + c_2/m^2$ relationship. The iterative solution adds more than 10% to the κ value of most of the crystals considered in our study, in both the ZZ and AC directions.

The ratio of thermal conductivity regarding each eigenvalue at each q-point is calculated using the ShengBTE code. However, these contributions are not listed in the mode resolved order, but are simply listed based on the ascending order of the frequency. Therefore, we can only resolve the con-

tribution of particular modes for a particular system as clearly seen in the phonon dispersions depicted in the ESI.† However, it can be certainly stated that the relative contributions of the listed first six modes (even if they get mixed in some regions) are almost temperature independent for all the materials when the temperature is slightly larger than the θ_D temperature computed using eqn (1). The total contributions of acoustic branches to the κ value are significantly higher than the contribution of optical modes as clearly seen for the materials, Bi, Sb, PSb, PBi, As Sb, *etc.*, in which acoustic modes distinctly separated from the rest.

The monolayers of group VA elements have significantly lower thermal conductivity compared to graphene, 2000–5000 W m^{-1} K^{-1}.[35,36] Due to the reflection symmetry perpendicular to in-plane and hexagonal symmetry, three-phonon scattering involving the ZA mode (anharmonic scattering of flexural phonons) process is significantly restricted in graphene, where any three-phonon processes involving an odd number of flexural phonon modes cannot occur.[37,38] The decreasing ZA contribution to the total thermal conductivity might be due to the fact that symmetry-based phonon–phonon scattering selection rules are broken in group VA monolayers.[14] The contribution of ZA modes, which can be distinctly separated from the rest as seen in the phonon dispersions depicted in the ESI,† to the total thermal conductivity decreases when moving from P to Bi. This can be associated with the degree of structural distortion (*i.e.* buckling in the sublayers) in the out of plane direction. While the bond angles (A_1 and A_2) are identical in the P and As monolayers, they are different for Sb and Bi, resulting in a different type of overlap between the orbitals within the sublayers for the latter monolayers. In addition, the compound monolayers with a large difference between the A_1 and A_2 angles were found to have smaller ZA contribution. Such structural distortion makes the transport path of phonons more tortuous.

The ZA mode behaves differently along the ZZ and AC directions. While the ZA mode provides a significant contribution to the total thermal conductivity along the ZZ direction for most of the monolayer structures, its contribution along the AC direction is usually smaller than 10% of the total conductivity. This can be explained in terms of distinct structural properties and strength of Umklapp scattering along the ZZ and AC directions. Phosphorene and other group VA monolayers were found to show superior structural flexibility along the AC direction allowing it to have large curvatures. This mechanical flexibility is the origin of less dispersive ZA, LA and TA modes along that direction. The quadratic behavior of the ZA mode is more apparent along this direction with a smaller group velocity. In graphene, the contribution of the ZA mode to κ is 80% of total conductivity. In general, the contribution of the ZA mode to κ is smaller than 50% in present systems. For all the considered materials, the thermal conductivity of the acoustic modes is more than 70% of the total thermal conductivity along the ZZ direction. LA and TA modes are always good heat carriers and provide significant contribution to the total thermal conductivity along both the ZZ and AC directions.

4. Conclusion

The lattice thermal transport properties of group VA monolayers (P, As, Sb, Bi, PAs, PSb, PBi, AsSb, AsBi, SbBi, P_3As_1, P_3Sb_1, P_1As_3, and As_3Sb_1), found to have no negative frequencies in their phonon dispersions, were systematically investigated using first-principles based calculations. In this manner, the effect of alloying on the lattice thermal transport properties of pristine P, As, Sb and Bi was estimated as well. Our calculations revealed that the κ values of all these monolayers can be correlated by their average atomic masses as follows: $\kappa(m) = c_1 + c_2/m^2$. In addition, the κ values of all the considered materials are almost inversely proportional to the temperature ($\kappa \sim T^{-1}$) for the T values ≥ 100 K and therefore the $\kappa(m) \sim m^{-2}$ correlation is clearly applicable for the same T range. Their anisotropic crystal structures give rise to significantly different phonon group velocities and peculiar scattering rates (phonon relaxation times) along the ZZ and AC directions, thereby anisotropic thermal conductivities. Using a simple formula developed by Slack,[48] we revealed that the anharmonic effects, which become stronger with an increase in the mass of constituent atoms, play an important role in lowering the thermal conductivity of these monolayers. Our investigations clearly point out that the thermal transport properties of phosphorene are tunable *via* substitutional Sb, As and Bi doping. For instance, the thermal conductivity of P along the ZZ direction, 109.6 W m^{-1} K^{-1}, can be suppressed as low as 10 W m^{-1} K^{-1}. Efficient thermoelectric applications demand materials with ultra-low thermal conductivity and good electrical conductivity. In this respect, we can propose PBi as a good candidate due to its ultra-low κ values along the AC direction, 1.5 W m^{-1} K^{-1}.

Conflicts of interest

There are no conflicts to declare.

Acknowledgements

References

1 H. Liu, A. T. Neal, Z. Zhu, Z. Luo, X. Xu, D. Tománek and P. D. Ye, *ACS Nano*, 2014, **8**, 4033–4041.
2 Z. Luo, J. Maassen, Y. Deng, Y. Du, R. P. Garrelts, M. S. Lundstrom, P. D. Ye and X. Xu, *Nat. Commun.*, 2015, **6**, 8572.

3 S. Zhang, Z. Yan, Y. Li, Z. Chen and H. Zeng, *Angew. Chem., Int. Ed.*, 2015, **54**, 3112–3115.

4 D. Çakır, H. Sahin and F. M. Peeters, *Phys. Rev. B: Condens. Matter Mater. Phys.*, 2014, **90**, 205421.

5 A. Chaves, T. Low, P. Avouris, D. Çakır and F. M. Peeters, *Phys. Rev. B: Condens. Matter Mater. Phys.*, 2015, **91**, 155311.

6 D. Çakır, C. Sevik and F. M. Peeters, *Phys. Rev. B: Condens. Matter Mater. Phys.*, 2015, **92**, 165406.

7 L. Li, Y. Yu, G. J. Ye, Q. Ge, X. Ou, H. Wu, D. Feng, X. H. Chen and Y. Zhang, *Nat. Nanotechnol.*, 2014, **9**, 372–377.

8 M. Zeraati, S. M. Vaez Allaei, I. Abdolhosseini Sarsari, M. Pourfath and D. Donadio, *Phys. Rev. B*, 2016, **93**, 085424.

9 G. Zheng, Y. Jia, S. Gao and S.-H. Ke, *Phys. Rev. B*, 2016, **94**, 155448.

10 L. Zhu, G. Zhang and B. Li, *Phys. Rev. B: Condens. Matter Mater. Phys.*, 2014, **90**, 214302.

11 H. O. H. Churchill and P. Jarillo-Herrero, *Nat. Nanotechnol.*, 2014, **9**, 330–331.

12 S. Wang, W. Wang and G. Zhao, *Phys. Chem. Chem. Phys.*, 2016, **18**, 31217–31222.

13 G. Wang, R. Pandey and S. P. Karna, *ACS Appl. Mater. Interfaces*, 2015, **7**, 11490–11496.

14 B. Peng, D. Zhang, H. Zhang, H. Shao, G. Ni, Y. Zhu and H. Zhu, *Nanoscale*, 2017, **9**, 7397.

15 D. Warschauer, *J. Appl. Phys.*, 1963, **34**, 1853–1860.

16 S. Zhang, M. Xie, F. Li, Z. Yan, Y. Li, E. Kan, W. Liu, Z. Chen and H. Zeng, *Angew. Chem.*, 2016, **128**, 1698–1701.

17 L. C. Hu, G. M. Ruan, T. C. Wei, C. J. Wang, Y. W. Lin, C. C. Lee, Y. Kawai and T. T. Li, *Thin Solid Films*, 2014, **570**, 574–579.

18 G. Kresse and J. Hafner, *Phys. Rev. B: Condens. Matter Mater. Phys.*, 1993, **47**, 558–561.

19 X. Wu, D. Vanderbilt and D. R. Hamann, *Phys. Rev. B: Condens. Matter Mater. Phys.*, 2005, **72**, 035105–035117.

20 R. W. Nunes and X. Gonze, *Phys. Rev. B: Condens. Matter Mater. Phys.*, 2001, **63**, 155107.

21 J. P. Perdew, K. Burke and M. Ernzerhof, *Phys. Rev. Lett.*, 1996, **77**, 3865–3868.

22 J. P. Perdew, K. Burke and M. Ernzerhof, *Phys. Rev. Lett.*, 1996, **77**, 3865–3868.

23 H. J. Monkhorst and J. D. Pack, *Phys. Rev. B: Solid State*, 1976, **13**, 5188–5192.

24 J. Ziman, *Electrons and Phonons: The Theory of Transport Phenomena in Solids*, Oxford University Press, 1960.

25 W. Li, J. Carrete, N. A. Katcho and N. Mingo, *Comput. Phys. Commun.*, 2014, **185**, 1747–1758.

26 W. Li, N. Mingo, L. Lindsay, D. A. Broido, D. A. Stewart and N. A. Katcho, *Phys. Rev. B: Condens. Matter Mater. Phys.*, 2012, **85**, 195436.

27 L. Lindsay, W. Li, J. Carrete, N. Mingo, D. A. Broido and T. L. Reinecke, *Phys. Rev. B: Condens. Matter Mater. Phys.*, 2014, **89**, 155426.

28 G. Qin, Q.-B. Yan, Z. Qin, S.-Y. Yue, H.-J. Cui, Q.-R. Zheng and G. Su, *Sci. Rep.*, 2014, **4**, 6946.

29 B. Peng, H. Zhang, H. Shao, Y. Xu, X. Zhang and H. Zhu, *RSC Adv.*, 2016, **6**, 5767–5773.

30 C. Kittel, *Introduction to Solid State Physics*, John Wiley & Sons, Inc., New York, 6th edn, 1986.

31 Y. Fujii, Y. Akahama, S. Endo, S. Narita, Y. Yamada and G. Shirane, *Solid State Commun.*, 1982, **44**, 579–582.

32 L. Lindsay, D. A. Broido and T. L. Reinecke, *Phys. Rev. Lett.*, 2013, **111**, 025901.

33 L. Lindsay, D. A. Broido and T. L. Reinecke, *Phys. Rev. Lett.*, 2012, **109**, 095901.

34 A. Jain and A. J. H. McGaughey, *J. Appl. Phys.*, 2014, **116**, 073503.

35 A. A. Balandin, *Nat. Mater.*, 2011, **10**, 569–581.

36 J. Haskins, A. Kınacı, C. Sevik, H. Sevinçli, G. Cuniberti and T. Çağın, *ACS Nano*, 2011, **5**, 3779–3787.

37 D. L. Nika and A. A. Balandin, *Rep. Prog. Phys.*, 2017, **80**, 036502.

38 D. L. Nika and A. A. Balandin, *J. Phys.: Condens. Matter*, 2012, **24**, 233203.

39 J. Carrete, N. Mingo and S. Curtarolo, *Appl. Phys. Lett.*, 2014, **105**, 101907.

40 A. Jain and A. J. H. McGaughey, *Sci. Rep.*, 2015, **5**, 8501 EP.

41 Y. Wang, G. Xu, Z. Hou, B. Yang, X. Zhang, E. Liu, X. Xi, Z. Liu, Z. Zeng, W. Wang and G. Wu, *Appl. Phys. Lett.*, 2016, **108**, 092102.

42 G. Qin, Q.-B. Yan, Z. Qin, S.-Y. Yue, M. Hu and G. Su, *Phys. Chem. Chem. Phys.*, 2015, **17**, 4854–4858.

43 T.-H. Liu and C.-C. Chang, *Nanoscale*, 2015, **7**, 10648–10654.

44 L. Cheng, H. J. Liu, J. Zhang, J. Wei, J. H. Liang, P. H. Jiang, D. D. Fan, L. Sun and J. Shi, *Phys. Chem. Chem. Phys.*, 2016, **18**, 17373–17379.

45 G. Qin, X. Zhang, S.-Y. Yue, Z. Qin, H. Wang, Y. Han and M. Hu, *Phys. Rev. B*, 2016, **94**, 165445.

46 L. Shulenburger, A. Baczewski, Z. Zhu, J. Guan and D. Tomanek, *Nano Lett.*, 2015, **15**, 8170–8175.

47 Z.-X. Hu, X. Kong, J. Qiao, B. Normand and W. Ji, *Nanoscale*, 2016, **8**, 2740–2750.

48 G. Slack, *J. Phys. Chem. Solids*, 1973, **34**, 321–335.

49 L.-D. Zhao, S.-H. Lo, Y. Zhang, H. Sun, G. Tan, C. Uher, C. Wolverton, V. P. Dravid and M. G. Kanatzidis, *Nature*, 2014, **508**, 373–377.

50 G. Zhang and B. Li, *Nanoscale*, 2010, **2**, 1058–1068.

51 Y. Zhou, Z.-X. Guo, H.-Y. Cao, S.-Y. Chen, H.-J. Xiang and X.-G. Gong, *Nanoscale*, 2016, **8**, 17815–17819.

52 C. Sevik, H. Sevinçli, G. Cuniberti and T. Çağın, *Nano Lett.*, 2011, **11**, 4971–4977.

53 L.-D. Zhao, C. Chang, G. Tan and M. G. Kanatzidis, *Energy Environ. Sci.*, 2016, **9**, 3044–3060.

54 J. O. Sofo and G. D. Mahan, *Phys. Rev. B: Condens. Matter Mater. Phys.*, 1994, **49**, 4565–4570.

55 D.-C. Zhang, A.-X. Zhang, S.-D. Guo and Y.-f. Duan, *RSC Adv.*, 2017, **7**, 24537–24546.

56 A. Ward, D. A. Broido, D. A. Stewart and G. Deinzer, *Phys. Rev. B: Condens. Matter Mater. Phys.*, 2009, **80**, 125203.